Matrix Infrared Spectra and Density Functional Theory Calculations of Manganese and Rhenium Hydrides

Xuefeng Wang and Lester Andrews*

Department of Chemistry, University of Virginia, Charlottesville, Virginia 22904-4319

Received: February 14, 2003; In Final Form: March 26, 2003

Laser-ablated Mn and Re atoms react with H_2 upon co-condensation in excess argon and neon and in pure hydrogen to produce metal hydrides. The reaction products are identified through isotopic substitution (D_2, HD, and $H_2 + D_2$) and density functional theory calculations. The $^7\Sigma^+$ ground state diatomic MnH is observed at 1493.3 cm^{-1} in solid neon, 1486.4 cm^{-1} in hydrogen, and 1477.9 cm^{-1} in argon. The ReH molecule gives a sharp band at 1985.0 cm^{-1} in argon, which is suggested to be the $^5\Sigma^+$ ground state by DFT calculations. The MnH_2 molecule provides ν_3 modes at 1600.8 cm^{-1} in solid neon, 1598.0 cm^{-1} in solid hydrogen, and 1592.3 cm^{-1} in solid argon, and the analogous ReH_2 molecule absorbs at 1646.4 cm^{-1} in solid argon. In addition MnH_2^- is observed at 1465.6 cm^{-1} in solid neon. The bonding properties of the first row transition metal dihydrides are compared, and reaction mechanisms of Mn and Re with H_2 are discussed. The novel ReH_4 molecule absorbs at 2037.2 and 590.6 cm^{-1}. This work reports the first experimental evidence for neutral rhenium hydride molecules.

Introduction

Neutral rhenium hydrides are unknown experimentally although a number of anion containing compounds such as Mg_3ReH_7, $BaReH_9$, $KNaReH_9$, and Rb_3ReH_{10} have been prepared in the solid state and structurally characterized by infrared spectra and neutron diffraction.[1−6] The nonahydrorhenate anion, ReH_9^{2-}, was the first soluble homoleptic hydrometalate to be unambiguously characterized.[6] Rhenium can also form classical and nonclassical hydride complexes, including octahedral ReH_6^{3-}, which are significant in organometallic chemistry and catalytic process.[7−9] The intensities of Re−H stretching vibrations in rhenium hydride complexes are extremely weak and are not observed spectroscopically. Finally, reactions of naked rhenium with molecular hydrogen have not yet been investigated experimentally although theoretical calculations have suggested that the Re(^{6}S) ground state does not insert into H_2 spontaneously.[10] Similar theoretical studies have been done for the reactions of rhodium with H_2, and a large energy barrier for insertion of ground state Rh(^{4}F) into H_2 was predicted,[11] but in contrast the spontaneous insertion was observed in low-temperature matrixes, where the spin−orbit coupling is believed to lower the reaction barrier.[12]

Reactions of several first and second row transition metal atoms with molecular hydrogen have been investigated in the gas phase and low-temperature noble gas matrix samples, which are fundamental to understanding bonding reactivity, and chemical properties of metal hydrides. Sweany has reviewed this earlier work.[13] For example, MnH_2 has been synthesized by co-condensing manganese and hydrogen atoms in solid argon[14] or Mn and H_2 followed by photolysis in solid xenon.[15] Similar experiments have been done with chromium.[16,17] The MnH_2 molecule was first proposed to be bent with a 117 ± 30° bond angle, but the same authors suggested in a later paper that the MnH_2 molecule might well be linear,[14,16] as found for FeH_2.[18,19] Hence, the structure of MnH_2 remains unclear.

The reactions of high-melting point metals with molecular hydrogen are difficult to investigate because these metal atoms cannot been generated by traditional thermal vaporization methods. Pulse-laser ablation is one of the most promising sources for high-melting metal atoms. A principle advantage of this technique is that more reactive metal atoms are produced in a very short time (10 ns) with very little heat load onto the cold matrix substrate during sample deposition. Using this method second and third row transition metal hydrides have been synthesized for infrared investigation.[12,20−26]

In this paper we report the reactions of laser-ablated rhenium and manganese atoms with molecular hydrogen in solid argon, neon, hydrogen, and deuterium during condensation at 3.5 K. The vibrational frequencies and structures of rhenium and manganese hydrides are determined using isotopic substitution in infrared spectra and density functional theory (DFT) calculations. This is the first observation of neutral rhenium hydride molecules. Finally, the reaction mechanisms and the nature of the bonding for the first row metal dihydrides are discussed.

Experimental and Computational Methods

The matrix infrared experiments for reactions of laser-ablated manganese and rhenium atoms with small molecules have been described in detail previously.[27−29] Laser-ablated metal atoms from manganese (Johnson Matthey) or rhenium (Goodfellow) targets were co-deposited with H_2, D_2, and HD in excess neon, argon, and pure hydrogen and deuterium at 3.5 K using a Sumitomo Heavy Industries RDK-205D Cryocooler. The Nd:YAG laser fundamental (1064 nm, 10 Hz repetition rate with 10 ns pulse width) was used and the laser energy was varied from 20 to 40 mJ/pulse. Normal hydrogen and deuterium (Matheson), HD (Cambridge Isotopic Laboratories), and selected mixtures were used in different experiments. FTIR spectra were recorded at 0.5 cm^{-1} resolution on a Nicolet 750 with 0.1 cm^{-1} accuracy using an MCTB detector. Matrix samples were annealed at different temperatures, and selected samples were

* Corresponding author. Electronic mail: lsa@virginia.edu.

10.1021/jp034392i CCC: $25.00
Published on Web 04/30/2003

TABLE 1: Infrared Absorptions (cm^{-1}) Observed from Reactions of Manganese and Rhenium with Dihydrogen in Excess Argon, Neon, Hydrogen, and Deuterium

argon			neon			pure solid		
H_2	HD	D_2	H_2	HD	D_2	H_2	D_2	identification
				Mn + H_2				
						3191.7	2303.7	MnH_2 ($\nu_1 + \nu_3$)
						2916.9	2118.4	MnH (2ν)
			1636		1177	1633.7	1174.1	(H_2MnH)
1592.3	1615.5, 1161.6	1155.1	1600.8	1621.7 1166.7	1159.4	1598.0	1157.1	MnH_2
1539		1116	1544	1552 1120	1109			(Mn_x- -MnH_2)[a]
1477.9	1477.9 1066.0	1066.0	1493.3	1493.3 1077.2	1077.2	1486.4	1072.7	MnH
			1465.6	1517.0 1093.8	1073.8			MnH_2^-
			1344		979	1334.9	969.1	Mn_2H_4
1162.0		849.7	1162.6	1120.0	847.4	1161.6	845.9	((MnH)$_2$)[a]
			1089.7		786.1			?
			877.4	876.0	875.0			((H_2)MnO)[a]
				Re + H_2				
2037.3	2037.2 2043.8 1460.0 1465.0	1459.4						ReH_4
1985.0	1985.0 1423.7	1423.5						ReH
			1977.0		1426.6		1428.0	Re_xH_y
1848.4		1330.8	1864.7		1341.4		1340.5	$Re_xH_y^-$
1648.4		1184.6						ReH_2 (site)
1646.4	1748.2 1232.1	1182.6						ReH_2
590.6								ReH_4

[a] Tentative.

subjected to photolysis by a medium-pressure mercury arc lamp (Phillips, 175 W) with globe removed.

Density functional theoretical calculations determined the structures and frequencies of expected manganese hydrides and rhenium hydrides using the Gaussian 98 program.[30] The BPW91 and B3LYP functionals,[31−34] the 6-311++G(d,p) basis set for H atom,[35] modified Wachters and Hay all-electron set for manganese atom,[36] and SDD pseudopotential for rhenium atom were employed.[37] All the geometrical parameters were fully optimized and the harmonic vibrational frequencies were obtained analytically at the optimized structures.

Results

Infrared spectra are presented for manganese and rhenium atom reactions with H_2, D_2, $H_2 + D_2$, and HD in excess argon, neon, and pure deuterium, and absorptions for reaction products are listed in Table 1. Density functional theoretical calculations of manganese and rhenium hydrides and hydrogen complexes assist in the identification of these molecules.

Infrared Spectra of Mn + H_2. Manganese atoms react with H_2 during condensation in excess neon at 3.5 K to give product absorptions at 1600.8, 1493.3, 1465.6, and 1162.6 cm^{-1}. These bands exhibited different behavior on $\lambda > 380$ nm and $\lambda > 240$ nm photolysis. With D_2 substitution the bands shift to 1159.4, 1077.2, 1073.8, and 847.4 cm^{-1} (Figures 1 and 2). Mixed $H_2 + D_2$ gave the same H_2 and D_2 bands, and the HD reaction exhibited strong new features in the upper Mn−H stretching region at 1621.7 cm^{-1} and the lower Mn−D stretching region at 1166.7 cm^{-1}.

In the argon matrix two major bands at 1592.3 and 1477.9 cm^{-1} observed after deposition increased on annealing to 15 and 25 K and shifted to 1155.1 and 1066.0 cm^{-1} with D_2 (Figure 3). Substitution with HD gave new bands at 1615.5 and 1161.6 cm^{-1} and the same 1477.9 and 1066.0 features as listed in Table 1. A weak band at 1663.3 cm^{-1} is due to HMnOH from the reaction of trace H_2O with manganese atom,[38] and a very weak 833.3 cm^{-1} band ($A = 0.001$) is due to MnO probably from surface oxide on the target.[39] Finally, the Ar_nH^+ and Ar_nD^+ bands were observed at 903.1 and 643.0 cm^{-1} in these experiments.[40]

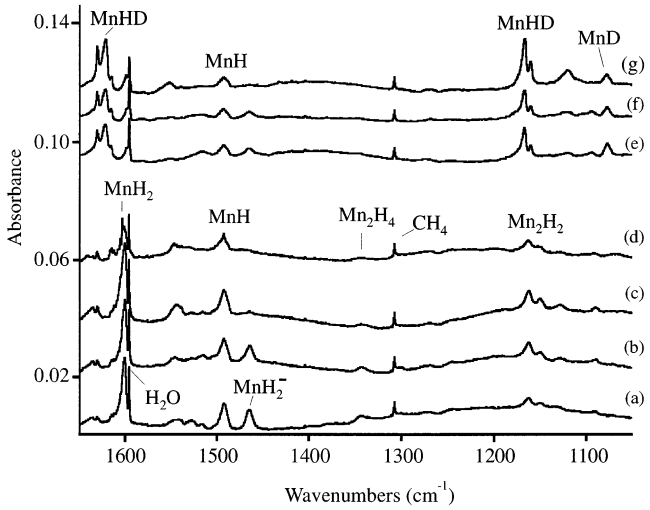

Figure 1. Infrared spectra in the 1650−1050 cm^{-1} region for laser-ablated Mn co-deposited with H_2 or HD in excess neon at 3.5 K: 3% H_2 in neon and Mn (a) co-deposited for 50 min, (b) after $\lambda > 380$ nm photolysis, (c) after 240−380 nm photolysis, and (d) after annealing to 11 K; 3% HD in neon and Mn (e) co-deposited for 50 min, (f) after annealing to 7.5 K, and (g) after 240−380 nm photolysis.

In the pure deuterium matrix a strong 1157.1 cm^{-1} band with 1174.1 and 1163.8 cm^{-1} satellites and 1072.7 cm^{-1} absorption

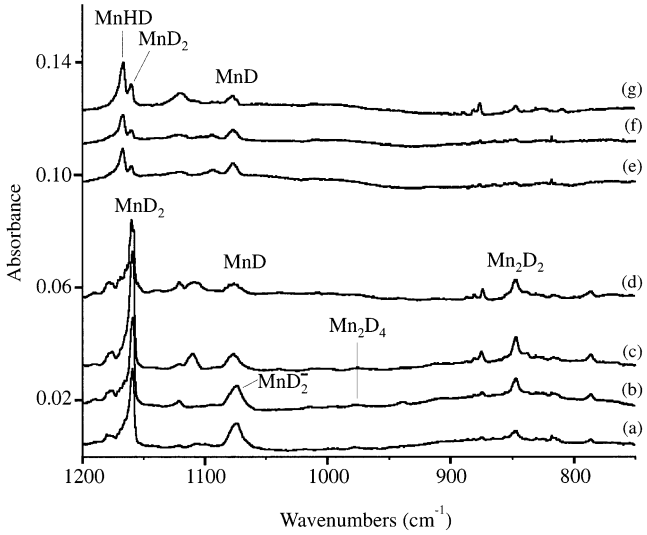

Figure 2. Infrared spectra in the 1200−750 cm^{-1} region for laser-ablated Mn co-deposited with D_2 or HD in excess neon at 3.5 K: 3% D_2 in neon and Mn (a) co-deposited for 50 min, (b) after $\lambda > 380$ nm photolysis, (c) after 240−380 nm photolysis, and (d) after annealing to 11 K; 3% HD in neon and Mn (e) co-deposited for 50 min, (f) after annealing to 7.5 K, and (g) after 240−380 nm photolysis.

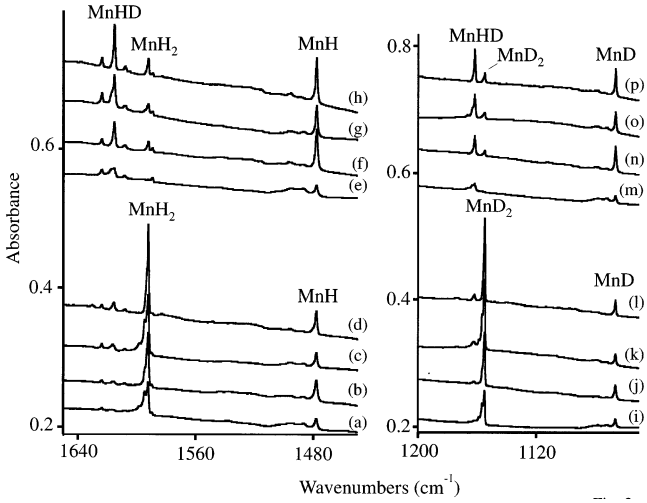

Figure 3. Infrared spectra in the 1650−1450 and 1200−1050 cm^{-1} regions for laser-ablated Mn co-deposited with H_2, D_2, and HD in excess argon at 3.5 K: 3% H_2 in argon and Mn (a) co-deposited for 50 min, (b) after annealing to 16 K, (c) after $\lambda > 240$ nm photolysis, and (d) after annealing to 25 K; 2% HD in argon (e) co-deposited for 50 min, (f) after annealing to 20 K, (g) after 240−380 nm photolysis, and (h) after annealing to 30 K; 3% D_2 in argon (i) co-deposited for 50 min, (j) after annealing to 16 K, (k) after $\lambda > 240$ nm photolysis, and (l) after annealing to 25 K; 2% HD in argon (m) co-deposited for 50 min, (n) after annealing to 20 K, (o) after $\lambda > 240$ nm photolysis, and (p) after annealing to 30 K.

are dominant (Figure 4). The 1157.1 cm^{-1} band doubled intensity on $\lambda > 380$ nm photolysis. Other bands at 2303.7, 2118.4, 969.1, and 845.9 cm^{-1} were also observed in this sample. The corresponding pure hydrogen experiment employed lower laser energy, and the weaker product bands (Figure 4) are listed in Table 1.

Infrared Spectra of Re + H_2. Reactions of rhenium atoms with H_2 in excess argon gave strong absorption at 1646.4 cm^{-1} with a 1660.8 cm^{-1} satellite and a weak band at 1985.0 cm^{-1} (Figure 5). Deuterium counterparts appeared at 1182.6 and 1423.5 cm^{-1} (Figure 6). Annealing to 15 K increased the 1985.0 cm^{-1} band, slightly decreased the 1646.4 cm^{-1} band, and produced a new band at 2037.2 cm^{-1}, which shifted to 1459.4

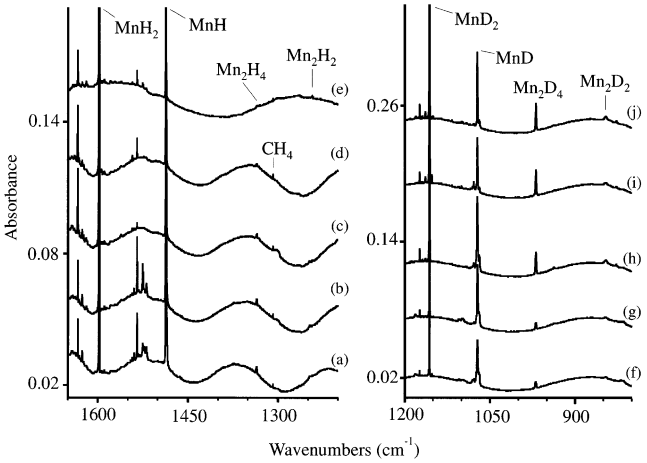

Figure 4. Infrared spectra in the 1650−1200 and 1200−800 cm^{-1} regions for laser-ablated Mn co-deposited with pure normal H_2 or D_2 at 3.5 K: Mn (a) co-deposited with 60 STPcc of H_2, (b) after annealing to 6.2 K, (c) after $\lambda > 380$ nm photolysis, (d) after 240−380 nm photolysis, and (e) after annealing to 6.4 K; Mn (f) co-deposited with 60 STP cc of D_2, (g) after annealing to 7.5 K, (h) after $\lambda > 380$ nm photolysis, (i) after 240−380 nm photolysis, and (j) after annealing to 8.5 K.

cm^{-1} with D_2. UV photolysis reversed the band intensities, i.e., increased the 1646.4 cm^{-1} band and decreased the 1985.0 and 2037.2 cm^{-1} bands. Experiments with $H_2 + D_2$ gave the same major bands, but with HD the 1646.4 cm^{-1} band (Re−H stretching region) shifted to 1748.2 cm^{-1} and the 1182.6 cm^{-1} band (Re-D stretching region) to 1232.1 cm^{-1} (Figures 5 and 6).

The reaction products trapped in neon and pure deuterium are complicated. Two broad bands at 1977.0 and 1864.7 cm^{-1} in the Re−H region and at 1426.6 and 1341.4 cm^{-1} in Re−D region were observed in a neon matrix. These bands are not significantly changed on annealing and photolysis. The product bands observed at 1428.0 and 1340.5 cm^{-1} in pure deuterium are comparable to neon bands. Finally, only very weak absorption was detected near 941 cm^{-1} for ReO_2, which indicates minimum sample contamination.[41]

Calculations. DFT calculations are done for manganese and rhenium hydrides, and the results are summarized in Tables 2−6. The ground state of MnH is predicted to be $^7\Sigma^+$ at the B3LYP/6-311++G(d,p) level of theory, and the computed 1.733 Å bond length and 1525.6 cm^{-1} Mn−H stretching frequency are close to the gas-phase experimental values of 1.731 Å and 1548.0 cm^{-1} (harmonic) and 1490.4 cm^{-1} (anharmonic), respectively.[42−46] This is in agreement with previous ab initio calculations on MnH.[47,48] At the same level the $^5\Sigma^+$ state is 19.6 kcal/mol higher in energy, the Mn−H bond length is reduced by 0.14 Å, and the frequency is increased to 1612.4 cm^{-1}. BPW91/6-311++G-(d,p) calculations also give very good predications for the Mn−H bond length and stretching frequency for the $^7\Sigma^+$ electronic state; however, the predicted total energies for both $^7\Sigma^+$and $^5\Sigma^+$ are very close (0.2 kcal/mol difference). The larger 6-311++G(3df,3pd) basis set gives basically the same results for both functionals.

For ReH the ground state is predicted to be $^5\Sigma^+$ at both B3LYP and BPW91 levels of theory, and the $^7\Sigma^+$ electronic state lies respectively 22.7 kcal/mol (B3LYP) and 16.1 kcal/mol (BPW91) higher in energy. This is in agreement with one but not another previous calculation on ReH.[49,50] Significantly the calculated frequencies for the two states are substantially different: $^5\Sigma^+$ values are near 2100 cm^{-1} with $^7\Sigma^+$ values near

TABLE 2: Bond Lengths, Vibrational Frequencies, and Intensities Calculated for MnH, MnH^-, and ReH

method	state bond (Å)	relative energy (kcal/mol)	frequencies, cm^{-1} (intensities, km/mol)
	MnH		
BPW91/6-311++G(d,p)	$^7\Sigma^+$, 1.710	0.0	MnH: 1548.3 (540)
			MnD: 1105.1 (275)[a]
	$^5\Sigma^+$, 1.590	−0.2	MnH: 1739.1 (20)
			MnD: 1241.2 (10)
BPW91/6-311++G(3df,3pd)	$^7\Sigma^+$, 1.711	0.0	MnH: 1522.0 (528)
			MnD: 1086.3 (269)
	$^5\Sigma^+$, 1.588	−0.2	MnH: 1727.5 (17)
			MnD: 1233.0 (9)
B3LYP/6-311++G(d,p)	$^7\Sigma^+$, 1.733	0.0	MnH: 1525.6 (506)
			MnD: 1088.9 (258)
	$^5\Sigma^+$, 1.590	+19.6	MnH: 1612.4 (195)
			MnD: 1150.8 (99)
B3LYP/6-311++G(3df,3pd)	$^7\Sigma^+$, 1.735	0.0	MnH: 1507.0 (496)
			MnD: 1075.6 (253)
	$^5\Sigma^+$, 1.644	+19.0	MnH: 1604.5 (189)
			MnD: 1145.2 (96)
	MnH^-		
BPW91/6-311++G(d,p)	$^6\Sigma^+$, 1.722	−26.5	MnH^-: 1334. (825)
			MnD^-: 952.2 (405)[b]
B3LYP/6-311++G(d,p)	$^6\Sigma^+$, 1.760	−23.4	MnH^-: 1276.4 (1006)
			MnD^-: 911.0 (495)
	ReH		
BPW91/6-311++G(d,p)/SDD	$^5\Sigma^+$, 1.644	0.0	ReH: 2099.1 (22)
			ReD: 1488.8 (11)[c]
	$^7\Sigma^+$, 1.798	+16.1	ReH: 1602.1 (643)
			ReD: 1136.3 (324)[d]
BPW91/6-311++G(3df,3pd)/SDD	$^5\Sigma^+$, 1.642	0.0	ReH: 2092.3 (20)
			ReD: 1484.0 (10)
	$^7\Sigma^+$, 1.797	+15.5	ReH: 1613.1 (633)
			ReD: 1144.1 (318)
B3LYP/6-311++G(d,p)/SDD	$^5\Sigma^+$, 1.641	0.0	ReH: 2110.0 (28)
			ReD: 1496.6 (14)
	$^7\Sigma^+$, 1.813	+22.7	ReH: 1545.1 (648)
			ReD: 1095.9 (326)
B3LYP/6-311++G(3df,3pd)/SDD	$^5\Sigma^+$, 1.640	0.0	ReH: 2101.6 (25)
			ReD: 1490.6 (13)
	$^7\Sigma^+$, 1.812	+22.3	ReH: 1559.6 (637)
			ReD: 1106.2 (321)

[a] $\langle s^2 \rangle$ after annihilation is 12.0000. [b] $\langle s^2 \rangle$ after annihilation is 8.7500. [c] $\langle s^2 \rangle$ after annihilation is 6.0002. [d] $\langle s^2 \rangle$ after annihilation is 12.0000.

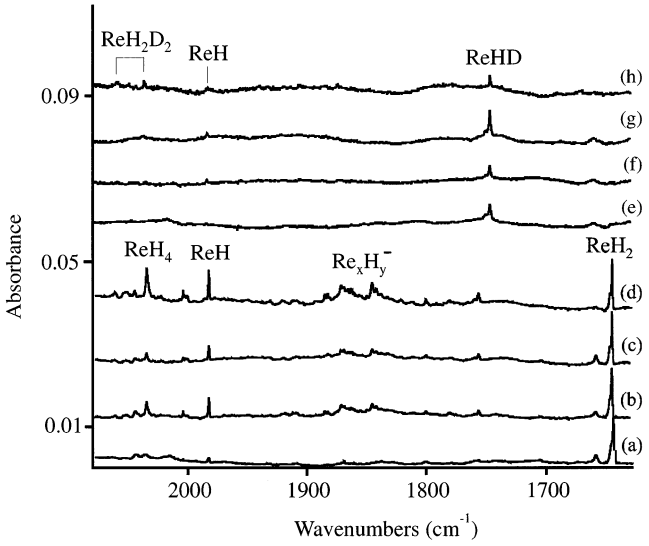

Figure 5. Infrared spectra in the 2080−1630 cm^{-1} region for laser-ablated Re co-deposited with H_2 or HD in excess argon at 3.5 K: 2% H_2 in argon and Re (a) co-deposited for 50 min, (b) after annealing to 15 K, (c) after $\lambda > 240$ nm photolysis, and (d) after annealing to 25 K; 3% HD in argon and Re (e), (f) after annealing to 15 K, (g) after $\lambda > 240$ nm photolysis, and (h) after annealing to 30 K.

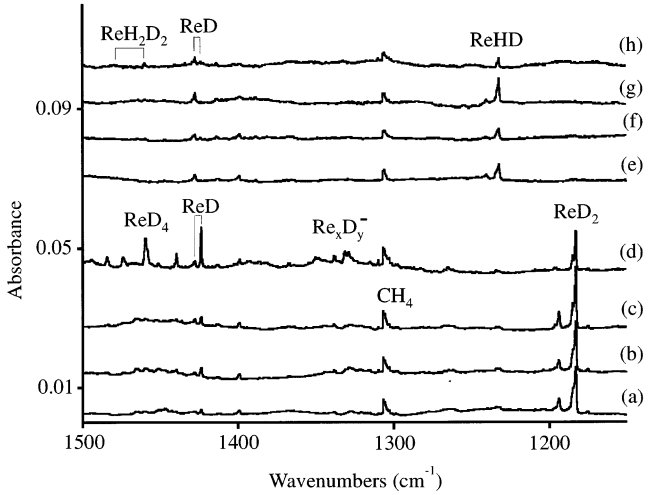

Figure 6. Infrared spectra in the 1500−1150 cm^{-1} region for laser-ablated Re co-deposited with D_2 or HD in excess argon at 3.5 K: 2% D_2 in argon and Re (a) co-deposited for 50 min, (b) after annealing to 17 K, (c) after $\lambda > 240$ nm photolysis, and (d) after annealing to 25 K; 3% HD in argon and Re (e), (f) after annealing to 15 K, (g) after $\lambda > 240$ nm photolysis, and (h) after annealing to 30 K.

1600 cm^{-1}. The $\langle s^2 \rangle$ expectation values (Table 2) are appropriate for the states calculated.

The manganese and rhenium dihydrides were computed at the same levels of theory. The MnH_2 molecule is predicted to be the $^6A_1$ ground state with a 1.669 Å Mn−H bond length and

TABLE 3: Geometries, Vibrational Frequencies, and Intensities Calculated for MnH_2 and MnH_2^-

method	state	relative energy (kcal/mol)	geometry (Å, deg)	frequencies, cm^{-1} (modes; intensities, km/mol)
BPW91	$^6A_1$	0.0	MnH: 1.669 HMnH: 156.2	MnH_2: 1691.2 (a_1; 17), 1625.3 (b_2; 646), 413.4 (a_1; 184) MnD_2: 1197.7 (9), 1169.0 (335), 297.2 (95) MnHD: 1659.2 (309), 1182.7 (195), 359.9 (140)
	$^6\Sigma_g^+$	0.6	MnH: 1.681	MnH_2: 1695.3 (σ_g; 0), 1602.0 (σ_u; 867), 365.0i (π_u; 306 × 2)
	$^4B_2$	28.7	MnH: 1.571 HMnH: 107.8	MnH_2: 1805.9 (a_1; 46), 1796.5 (b_2; 160), 718.7 (a_1; 68)
	$^4A_1$	38.6	MnH: 1.659 HMnH: 160.1	MnH_2: 1716.9 (a_1; 9), 1388.5 (b_2; 7954), 387.9 (a_1; 190)
	$^5\Sigma_g^+$	−18.3	MnH: 1.694 HMnH: 180.0	MnH_2^-: 1548.6 (σ_g; 0), 1402.6 (σ_u; 451), 359.6 (π; 2 × 5) MnD_2^-: 1095.5 (0), 1009.6 (218), 258.8 (2 × 5) $MnHD^-$: 1483.5 (184), 1044.9 (150), 313.9 (2 × 5)
B3LYP[a]	$^6\Sigma_g^+$	0.0	MnH: 1.692	MnH_2: 1697.3 (σ_g; 0), 1621.2 (σ_u; 759), 240.8 (π_u; 339 × 2) MnD_2: 1200.8 (0), 1167.0 (397), 173.2 (175 × 2) MnHD: 1661.0 (350), 1182.4 (227), 209.9 (257)
	$^4B_2$	38.1	MnH: 1.579 HMnH: 111.7	MnH_2: 2352.9 (b_2; 1887), 1782.6 (a_1; 55), 741.2 (a_1; 69)
	$^4A_2$	44.3	MnH: 1.592 HMnH: 102.9	MnH_2: 1847.2 (b_2; 115), 1772.4 (a_1; 52), 593.1 (a_1; 68)
	$^5A_1$	−17.3	MnH: 1.689 HMnH: 165.4	MnH_2^-: 1557.7 (a_1; 2), 1429.3 (b_2; 452), 396.7 (a_1; 11) MnD_2^-: 1102.1 (1), 1028.5 (218), 285.5 (8) $MnHD^-$: 1499.4 (191), 1059.6 (145), 344.2 (10)

[a] Basis set: 6-311++G(d,p) for H and Wachters-Hay for Mn.

TABLE 4: Geometries, Vibrational Frequencies, and Intensities Calculated for $ReH_2$and ReH_2^-

method	state	relative energy (kcal/mol)	geometry (Å, deg)	frequencies, cm^{-1} (modes; intensities, km/mol)
BPW91[a]	$^6A_1$	0.0	ReH: 1.745 HReH: 146.0	ReH_2: 1874.5 (a_1,43), 1717.7 (b_2; 463), 648.4 (a_1; 10) ReD_2: 1326.9 (22), 1221.0 (233), 460.7 (5) ReHD: 1803.6 (214), 1266.9 (167), 562.2 (8)
	$^6\Sigma_g^+$	3.3	ReH: 1.787	ReH_2: 1853.7 (σ_g; 0), 1600.4 (σ_u; 1158), 745.5i (π_u; 243 × 2)
	$^4B_1$	7.3	ReH: 1.651 HReH: 112.5	ReH_2: 2073.7 (a_1; 27), 2061.3 (b_2; 86), 738.0 (a_1; 29)
	$^6\Sigma_u^+$	50.1	ReH: 1.770	ReH_2: 1672.9 (σ_g; 0), 1339.0 (σ_u; 1158), 793.6 (π_u; 243 × 2)
	$^5A_2$	−11.7	ReH: 1.768 HReH: 145.6	ReH_2^-: 2008.1 (b_2; 2008.1), 1696.2 (a_1; 137), 439.4 (a_1; 1)
B3LYP[a]	$^6A_1$	0.0	ReH: 1.753 HReH: 147.8	ReH_2: 1871.8 (a_1; 43), 1697.8 (b_2; 572), 586.5 (a_1; 24) ReD_2: 1325.0 (22), 1206.9 (289), 416.8 (12) ReHD: 1794.3 (253), 1257.0 (210), 508.4 (19)
	$^6\Sigma_g^+$	3.2	ReH: 1.787	ReH_2: 1865.6 (σ_g; 0), 1597.1 (σ_u; 1160), 583.7i (π_u; 226 × 2)
	$^4B_2$	−1.4	ReH: 1.648 HReH: 114.1	ReH_2: 2107.9 (b_2; 138), 2098.5 (a_1; 42), 801.8 (a_1; 23)
	$^6\Sigma_u^+$	47.3	ReH: 1.770	ReH_2: 1680.5 (σ_g; 0), 1331.1 (σ_u; 1150), 802.2 (π_u; 3 × 2)

[a] Basis set: 6-311++G(d,p) and SDD pseudopotential for Re.

with a slightly bent 156.2° H−Mn−H bond angle at the BPW91/6-311++G(d,p) level (Table 3). Linear MnH_2 ($^6\Sigma_g^+$) is calculated to be only 0.6 kcal/mol higher in energy, but imaginary frequencies are found for the degenerate H−Mn−H bending mode. Two bent quartet MnH_2 structures lie 28.7 and 38.6 kcal/mol higher in energy. With the B3LYP functional only the linear $^6\Sigma_g^+$ ground state is located for MnH_2, in agreement with early and recent reports,[51,52] and the two quartet states lie much higher in energy. Finally, very recent CCSD calculations find MnH_2 to be linear.[53]

Similar calculations are reported for ReH_2 with the BPW91 and B3LYP functionals (Table 4). With the SDD pseudopotential employed for Re, the $^6A_1$ state with a 146.0° H−Re−H bond angle is predicted to be the ground state, and the linear $^6\Sigma_g^+$ state with imaginary bending frequencies is about 3 kcal/mol higher in energy. Another linear $^6\Sigma_u^+$ state is found with real frequencies, but it is 50 kcal/mol higher in energy.

Higher manganese hydrides are calculated to provide a guide for reaction products as H_2 moieties are associated with MnH and MnH_2 (Table 5). The hydrogen complexes, $(H_2)MnH$ and $(H_2)MnH_2$, are obtained instead of MnH_3 and MnH_4, respectively, as found in calculations for V and Cr hydrides.[54,55] The BPW91 functional predicts that $^5B_1$, $^5A_1$, and $^5A_2$ $(H_2)MnH$ states are 11−22 kcal/mol higher than the $^5B_2$ state. The B3LYP functional gives similar results in that $^5B_2$ is the ground state by 3 kcal/mol over H_2 + MnH and 3−20 kcal/mol over the above three $(H_2)MnH$ states. Note that the total energy of (H_2)-MnH is lower than that of MnH + H_2 but that $(H_2)MnH_2$ is higher than MnH_2 + H_2. Because the MnH_2 molecule is a sextet state, sextet states for $(H_2)MnH_2$ are computed but these are repulsive. More rigorous CCSD calculations find a C_{2v} H_2MnH molecule.[53] The higher rhenium hydrides, ReH_3 (C_s) and ReH_4 (D_{2d}), are computed at the same levels of theory starting with dihydrogen complexes (Table 6), and in contrast, hydride structures are converged. ReH_4 is slightly distorted from tetrahedral symmetry in the $^2A_1$ ground state at the DFT level, and the $^4A_2$ state is slightly higher in energy.

States for the dimanganese species Mn_2H_2 and Mn_2H_4 were calculated with BPW91; an $^{11}A_g$ rhombic ring $(MnH)_2$ was 5 kcal/mol more stable than the two nonet states. The Mn_2H_4 molecule converged to a stable nonet spin state D_{2d} structure with real frequencies (Table 5), a 2.17 Å Mn−Mn bond, 124.6° H−Mn−H angles, a short Mn−H_2 distance of 1.680 Å, and a long MnH_2 distance of 2.040 Å.

TABLE 5: Geometries, Vibrational Frequencies, and Intensities Calculated for Higher Mangenese Hydrides at the BPW91 Level[a]

molecule	state	relative energy (kcal/mol)	geometry (Å, deg)	frequencies, cm^{-1} (modes, intensities, km/mol)
$(H_2)MnH$ (C_{2v})	$^5B_2$	−11[b]	MnH: 1.641 MnH′: 1.693 H′H′: 0.940	2126 (a_1; 556), 1699 (a_1; 205), 1608 (b_2; 18), 955 (a_1; 41), 504 (b_2; 77), 301 (b_1; 131)
$(H_2)MnH_2$ (C_{2v})	$^4A_2$	+15.0[c]	MnH: 1.619 MnH′: 1.620 HH: 1.025 H′H′: 1.026	1897.9 (a_1; 544), 1817.9 (a_1; 0), 1781.2 (b_1; 31), 1778.6 (b_2; 31), 1006.8 (a_2; 0), 959.2 (a_1; 0), 675.1 (a_1; 812), 454.3 (b_2; 22); 454.1 (b_1, 22)
$(MnH)_2$ (C_{2h})	$^{11}A_g$	−46[d]	MnH: 1.843 HMnH: 96.6	1284 (a_u; 75), 1232 (a_g; 0), 1148 (b_u; 144) 753 (a_g; 0), 421 (b_u; 112), 269 (a_g; 0)
Mn_2H_4 (D_{2d})	^9X	−13[e]	MnH: 1.680 MnMn: 2.176 HMnH: 124.6 Mn′H: 2.040	1539 (a_1; 0), 1526 (b_2; 19), 1463 (e; 237 × 2) 763 (b_1; 0), 605 (e; 6 × 2), 476 (a_1; 0) 299 (a_1; 0), 286 (b_2; 228), 259 (e; 12 × 2) [1091 (0), 1081 (10), 1048 (120)][f] [1533 (10), 1462 (237), 1086 (5), 1049 (120)][g] [1503 (110), 1495 (125), 1069 (69), 1065 (68)][h]

[a] Basis set: Wachters−Hay for Mn and 6-311++G(d,p) for H. [b] Energy relative to H_2 + MnH. [c] Energy relative to H_2 + MnH_2. [d] Energy relative to 2 MnH. [e] Energy relative to 2 MnH_2. [f] Mn_2D_4. [g] MnH_2MnD_2. [h] MnHDMnHD.

TABLE 6: Geometries, Vibrational Frequencies, and Intensities Calculated for ReH_3 and ReH_4[a]

molecule (symm)	state	relative energy (kcal/mol)	geometry (Å, deg)	frequencies, cm^{-1} (modes, intensities, km/mol)
			BPW91/6-311++G(d,p)/SDD	
ReH_3 (C_s)	$^3A'$	0.0	ReH: 1.645 ReH′: 1.649 H′ReH′: 111.6	ReH_3: 2114.8 (a′; 15), 2092.7 (a′; 78), 2091.2 (a″; 82) 725.9 (a′; 29), 490.0 (a′; 78), 312.7 (a″; 62) ReD_3: 1498.4 (9), 1484.9 (42), 1484.6 (39), 515.2 (15) 348.6 (39), 221.6 (31)
	$^5A'$	0.8	ReH: 1.646 ReH′: 1.740 H′ReH′:146.0	ReH_3: 2119.2 (a′; 34), 1891.3 (a′; 60), 1711.8 (a″; 438), 773.0 (a′; 6), 259.0 (a′; 76), 505.2i (a″; 1)
ReH_4 (D_{2d})	$^2A_1$	0.0	ReH: 1.649 HReH: 108.2	ReH_4: 2116.2 (a_1; 0), 2096.6 (e; 76 × 2), 2093.5 (b_2; 102) 777.5 (a_1; 0), 673.9 (b_2; 62), 626.0 (b_1; 0), 584.8 (e; 72 × 2) ReD_4: 1496.9 (0), 1489.1 (39 × 2), 1485.8 (52), 550.0 (0) 480.1 (31), 442.8 (0), 416.9 (37) ReH_2D_2: 2104.9 (49), 2096.0 (74), 1491.4 (28), 1489.9 (42) 734.2 (22), 547.7 (63), 541.1 (0), 506.5 (24), 462.1 (45)
	$^4A_2$	3.9	ReH: 1.691 HReH: 71.0	ReH_4: 2016.9 (a_1; 0), 1948.6 (e; 51 × 2), 1948.5 (b_2; 166) 911.9 (b_1; 0), 507.5 (a_1; 0), 467.5 (e; 27 × 2), 452.7 (b_2; 45)
			B3LYP/6-311++G(d,p)/SDD	
ReH_3 (C_s)	$^3A'$	0.0	ReH: 1.652 ReH′: 1.640 HReH′: 110.4 H′ReH′:86.6	ReH_3: 2145.1 (a′; 55), 2116.1 (a″; 63), 2102.9 (a′; 133) 698.8 (a″; 21), 684.8 (a′; 69), 341.1 (a′; 12) ReD_3: 1521.8 (33), 1500.8 (32), 1491.9 (63), 495.5 (11) 486.6 (35), 242.0 (6)
	$^5A'$	1.0	ReH: 1.646 ReH′: 1.745 HReH′: 106.2 H′ReH′:147.6	ReH_3: 2130.3 (a′; 50), 1900.9 (a′; 67), 1708.1 (a″; 568), 732.5 (a′; 13), 227.9 (a′; 113), 486.3i (a″; 2)
ReH_4 (D_{2d})	$^2A_1$	0.0	ReH: 1.649 HReH: 110.5	ReH_4: 2146.2 (a_1; 0), 2120.8 (b_2; 152), 2119.2 (e; 120 × 2) 769.6 (a_1; 0), 643.6 (b_2; 76), 600.2 (e; 84 × 2), 527.0 (b_1; 0) ReD_4: 1518.2 (0), 1505.6 (62 × 2), 1505.5 (78), 544.4 (0) 458.4 (39), 427.3 (43 × 2), 372.8 (0) ReH_2D_2: 2133.6 (74), 2119.3 (117), 1511.9 (41), 1506.6 (65), 719.4 (25), 560.9 (73), 488.7 (32), 476.2 (53) 455.2 (0)
	$^4A_2$	4.9	ReH: 1.688 HReH: 75.9	ReH_4: 2043.1 (a_1; 0), 1989.2 (b_2; 200), 1953.7 (e; 86 × 2) 879.1 (b_1; 0), 582.9 (a_1; 0), 475.5 (b_2; 19), 396.2 (e; 47 × 2)

[a] Basis set: 6-311++G(d,p) and SDD pseudopotential for Re.

Finally, the MnH^-, MnH_2^-, and ReH_2^- molecular anions were computed, and these are also listed in the tables.

Discussion

The new product absorptions will be identified and assigned from isotopic shifts and comparison to DFT frequency calculations.

MnH. The sharp 1477.9 and 1066.0 cm^{-1} argon matrix bands observed for Mn with H_2 and D_2, respectively, increase on 20 K annealing, decrease slightly on $\lambda > 240$ nm photolysis, restore on 25 K annealing, and then decrease on subsequent annealing. Precisely the same bands are observed with the HD reagent, which demonstrates that a single H(D) atom is involved and indicates the MnH and MnD assignments. The MnH/MnD =

1477.9/1066.0 = 1.3864 ratio is appropriate for a metal-hydride vibration. Our observations are in agreement with the Weltner report[14] within experimental measurement error.

The MnH and MnD molecules exhibit a modest blue shift in solid neon to 1493.3 and 1077.2 cm^{-1}, respectively, (ratio 1.3863) (Figures 1 and 2). Again the same bands are observed with HD. In neon these bands decrease slightly on annealing to 9 K. The sharp 1072.7 cm^{-1} absorption in pure deuterium intermediate between the argon and neon matrix values is assigned to MnD with the pure hydrogen MnH counterpart at 1486.4 cm^{-1} (ratio 1.3859). Even though MnH is a high-spin ($^7\Sigma^+$) species, interaction with the hydrogen host is minimal.

Weaker bands at 2916.9 and 2118.4 cm^{-1} track with the stronger 1486.4 and 1072.7 cm^{-1} fundamental bands and are due to the corresponding overtones. The absorbances are 2916.9 (0.0038), 1486.4 (0.293), 2118.4 (0.0005), and 1072.7 cm^{-1} (0.060). The harmonic and anharmonic vibrational constants are therefore determined: $2 \times 1486.4 - 2916.9 = 55.9\ cm^{-1} = 2\omega_e x_e$ and $\omega_e = 1542.3\ cm^{-1}$ for MnH whereas $2 \times 1072.7 - 2118.4 = 27.0\ cm^{-1} = 2\omega_e x_e$ and $\omega_e = 1099.7\ cm^{-1}$ for MnD. These constants are slightly smaller than gas-phase values: for MnH solid H_2 red shifts ω_e by 5.7 cm^{-1} (0.37%) and $\omega_e x_e$ by 0.8 cm^{-1} (2.7%), and for MnD solid D_2 red shifts ω_e by 2.8 cm^{-1} (0.25%) and $\omega_e x_e$ by 0.4 cm^{-1} (2.9%). Hence the H_2 (D_2) matrix environment affects the anharmonic potential constant relatively more than the harmonic potential constant.

The matrix assignments for MnH are in accord with the gas-phase[42] fundamental frequency, 1490.4 cm^{-1}, where the neon matrix affects a 2.9 cm^{-1} blue shift, the hydrogen matrix a 4.0 cm^{-1} red shift, and the argon matrix a 12.5 cm^{-1} red shift. These modest matrix shifts are in line with vibrational frequency shifts for other molecules.[56] However, the larger red matrix shift in argon is in accord with the greater polarization and interaction of $^7\Sigma^+$ MnH with argon as described for the Fermi contact interaction.[44] Finally, the experimental MnH frequencies are in agreement with the prediction of the most recent quantum chemical calculations for the ground $^7\Sigma^+$ state, as described in a recent review.[48] The 1530 cm^{-1} MCPF value is representative.[47] Our BPW91 and B3LYP calculations (Table 2) find similar frequencies for MnH.

MnH_2. Infrared spectra of MnH_2 have been reported following photolysis of Mn and H_2 in solid xenon[15] and co-condensation of Mn and H atoms in excess argon.[14] The present argon matrix spectrum is in agreement with that of Weltner et al. except for 0.5−1.7 cm^{-1} differences in grating spectrometer measurement.[14] The identification of MnH_2 is confirmed by the spectra of MnHD and MnD_2. The MnH_2/MnD_2 antisymmetric stretching frequency ratio 1592.3/1155.1 = 1.3785 and the ratio for the Mn−H/Mn−D stretching modes of MnHD 1615.5/1161.6 = 1.3908 are both indicative of metal−hydride vibrations. The former antisymmetric mode is more anharmonic than the bond stretching modes in MnHD. The observation of two new absorptions with HD and their relationship to the strong MnH_2 and MnD_2 product bands demonstrates that two equivalent H(D) atoms are involved in the vibration. Thus the strong 1565 cm^{-1} band assigned to MnH_2 in solid xenon[15] sustains a large red shift by this polarizable medium. The weaker 1591 cm^{-1} absorption is probably due to MnH_2 molecules on surface sites with weaker matrix interactions.

Our neon matrix spectrum gives blue-shifted bands at 1600.8 cm^{-1} for MnH_2 and 1159.4 for MnD_2 (ratio 1.3807), and at 1621.7 and 1166.7 cm^{-1} for the Mn−H and Mn−D stretching modes of MnHD (ratio 1.3900). The appearance of MnHD absorptions above the antisymmetric modes of MnH_2 and MnD_2 points to the observation of a higher, unobserved symmetric mode. In the neon matrix case the symmetric mode is predicted for MnH_2 at $1601 + 2(1622 - 1601) = 1642\ cm^{-1}$ (the Mn−H mode for MnHD should be near the median of a_1 (σ_g) and b_2 (σ_u) MnH_2 modes).

Very strong absorptions at 1598.0 and 1157.1 cm^{-1} in pure H_2 and D_2, respectively, with ratio 1.3810, are shifted only 2.8 and 2.4 cm^{-1} from the above neon matrix values, and these bands are due to the antisymmetric stretching modes of MnH_2 and MnD_2 isolated in solid dihydrogen with little chemical interaction. The MnHD counterparts are observed at 1617.7 and 1163.8 cm^{-1} in pure D_2. The weaker 3191.7 and 2303.7 cm^{-1} absorptions track with the very strong absorptions (0.80 and 0.70% relative absorbance, respectively) and are assigned to the $\nu_1 + \nu_3$ combination bands of MnH_2 and MnD_2. As the ν_1 modes of MnH_2 and MnD_2 are deduced to be 42 and 18 cm^{-1} higher than the ν_3 modes in solid neon, and the $\nu_1 + \nu_3$ combination better accounts for the expected anharmonicity than a possible $2\nu_3$ overtone assignment. The lack of an obvious ν_1 fundamental is in accord with a linear MnH_2 molecule.

The identification of MnH_2 is further confirmed by quantum chemical calculations. First, MnH_2 is predicted to be linear at the CCSD(T) level in a $^6\Sigma_g^+$ state with 1646.5 cm^{-1} σ_g and 1608.9 cm^{-1} σ_u frequencies corrected for anharmonicity.[53] These calculated frequencies are extremely close to our 1642 and 1600.8 cm^{-1} neon matrix values. Second, our DFT calculations fit almost as well. The BPW91 method converges to a slightly bent (156.2°) $^6A_1$ state with uncorrected 1691.2 and 1625.3 cm^{-1} a_1 and b_2 harmonic frequencies, respectively, and the linear $^6\Sigma_g^+$ state is only 0.6 kcal/mol higher with uncorrected 1695.3 and 1602.0 cm^{-1} σ_g and σ_u frequencies (Table 3). The B3LYP calculation converges to a $^6\Sigma_g^+$ ground state with uncorrected 1697.3 and 1621.2 cm^{-1} harmonic frequencies.

MnH_2^-. The new 1465.6 cm^{-1} neon matrix band decreases slightly on annealing and is virtually destroyed by 240−380 nm photolysis. The photosensitive D_2 counterpart at 1073.8 cm^{-1} defines a 1465.6/1073.8 = 1.3649 ratio, which is slightly lower than the ratio (1.3807) for MnH_2. Photosensitive HD counterparts at 1517.0 and 1093.8 cm^{-1} are in accord with assignment to a MnH_2 vibration and the photolysis behavior suggests the MnH_2^- anion observed by 488 nm laser photodetachment in the gas phase.[57]

Our B3LYP calculations predict a strong antisymmetric stretching fundamental for a slightly bent $^5A_1$ ground state of MnH_2^- near 1430 cm^{-1}. This result is in general agreement with CCSD calculations, which describe a linear MnH_2^- anion with strong σ_u fundamental at 1488 or 1430 cm^{-1} depending on the basis set.[53] The agreement between calculated and observed frequencies invites assignment of the photosensitive 1465.6 cm^{-1} absorption to MnH_2^-.

The HD counterpart absorptions at 1517.0 and 1093.8 cm^{-1} strongly support this assignment. Our DFT calculations find the symmetric mode above the antisymmetric mode, and thus both stretching modes of $MnHD^-$ should be higher than the σ_u modes of MnH_2^- and MnD_2^-, as found for MnH_2 and MnD_2, but in the anion case the mode separations are larger. Our BPW91 calculation predicts the Mn−H and Mn−D stretching modes of $MnHD^-$ to be 73 and 32 cm^{-1} higher than the antisymmetric stretching modes of MnH_2^- and MnD_2^-, respectively, in excellent agreement with the observed 51 and 20 cm^{-1} separations. Thus, the unobserved σ_g mode of MnH_2^- is deduced to be $1466 + 2(51) = 1568\ cm^{-1}$ from observed frequencies. Finally, our DFT calculations estimate a 17−18 kcal/mol

electron affinity for MnH_2, which is slightly higher than the 10.2 kcal/mol experimental value.[57]

The slightly lower H/D frequency ratio for MnH_2^- as compared to MnH_2 implies greater anharmonicity in the vibration instead of a structural difference. Although our B3LYP calculation finds slightly bent species, recent CCSD computations give linear structures for both. High-resolution spectra of FeH_2, which is isoelectronic with MnH_2^-, characterize a linear molecule.[19]

Higher Manganese Hydrides. Four weak bands at 1636, 1544, 1344, and 1162.6 cm^{-1} in solid neon remain to be assigned. These bands increase on photolysis, which increases MnH and MnH_2 so dihydrogen complexes or aggregates of these molecules must be considered. Our DFT calculations find a (H_2)-MnH complex, but higher level calculations characterize a H_2-MnH hydride species with C_{2v} symmetry.[53] However, both predict the strongest infrared band in the high 1600 cm^{-1} region. Accordingly, we tentatively assign the 1636 cm^{-1} absorption to an H_2MnH species, which can reasonably be expected in this system.[14] A small yield of this product is observed in pure H_2 at 1633.7 cm^{-1}.

The 1544 cm^{-1} band exhibits the characteristics of a MnH_2 vibration: shift to 1109 cm^{-1} with D_2 (1.392 ratio) and higher HD counterparts at 1552 and 1120 cm^{-1}, analogous to MnHD. Our DFT calculations find $(H_2)MnH_2$ to have higher energy than H_2 and MnH_2. This is in line with our observation of MnH_2 and MnD_2 in solid H_2 and D_2, respectively, only 4−2 cm^{-1} lower than in solid neon, which shows that MnH_2 does not form a dihydrogen complex. The bent CrH_2 molecule, however, readily complexes with dihydrogen.[55] The 1544 cm^{-1} band increases on annealing and is tentatively assigned to a weak Mn_x-MnH_2 complex where the MnH_2 structure is essentially unchanged.

The broad 1344 and 979 cm^{-1} neon matrix absorptions exhibit sharper 1334.9 and 969.1 cm^{-1} solid hydrogen and deuterium counterparts, respectively. Photolysis ($\lambda > 380$ nm) increases the 1334.9 cm^{-1} band slightly and the 969.1 cm^{-1} band 3-fold. The H/D isotopic frequency ratios, 1.373 and 1.378 are appropriate for a MnH_2 vibration, and the large yield of MnH_2 in pure hydrogen and deuterium invites consideration of Mn_2H_4. Our DFT calculations find a stable D_{2d} structure with a very strong e mode at 1463 cm^{-1}, which, scaled by 0.92, fits the observed bands. Furthermore, the mixed isotopic pattern shows that four slightly coupled hydrogens are involved in this mode, and the four satellite bands fit the pattern computed for MnHDMnHD (Table 5). A 50/50 pure H_2/D_2 experiment gave strong new 1337.6 and 969.4 cm^{-1} bands with weaker 1350.9, 1367.8 cm^{-1} and 976.8, 982.3 cm^{-1} satellites, and the same pattern was observed with pure HD.

The 1162.6 cm^{-1} band is in the region expected for bridged hydrogen vibrations. This band shifts to 847.4 cm^{-1} with D_2 (H/D ratio 1.3720), but HD counterparts are masked by other absorptions. The calculation of $(MnH)_2$ is a formidable theoretical problem. Using BPW91, we find an $^{11}A_g$ ground state with the strongest infrared absorption at 1148 cm^{-1} and a weaker band at 1284 cm^{-1}. The 1162.6 cm^{-1} band is tentatively assigned to $(MnH)_2$.

ReH. The sharp bands for Re with H_2 and D_2 in argon at 1985.0 and 1423.5 cm^{-1}, respectively, increase on 15 K annealing, decrease on photolysis, and increase more on 25 K annealing (Figure 5), but decrease on final 30 K annealing (not shown). This behavior is analogous to that found for MnH in solid argon. With the HD reagent, the above bands were observed essentially unshifted, which indicates that a single H(D) atom is involved and suggests the ReH and ReD diatomic molecules. The H/D frequency ratio 1985.0/1423.5 = 1.3945 is slightly higher than found for MnH, which is appropriate for the vibration of H(D) against a heavier metal atom.

Assignment of the 1985.0 cm^{-1} solid argon band to ReH is supported by quantum chemical calculations. Both BPW91 and B3LYP calculations find the $^5\Sigma^+$ state lower than the $^7\Sigma^+$ state (by 16.1 and 22.7 kcal/mol, respectively), but the harmonic frequency is substantially higher, in the 2100 cm^{-1} region, for the $^5\Sigma^+$ state. This is consistent with the 1985.0 cm^{-1} fundamental in solid argon. Unfortunately, we are not able to isolate ReH or ReH_2 in solid neon: we believe the heat load on the condensing sample is too great for rapid freezing because higher laser energy is required to ablate Re than Mn. Although ReH has not yet been observed in the gas phase, the present argon matrix observations point to a gas-phase fundamental near 2000 cm^{-1} for the $^5\Sigma^+$ ground state.

ReH_2. The sharp 1646.4 and 1182.6 cm^{-1} bands for Re with H_2 and D_2 in argon show little change on 15 K annealing, increase slightly on broadband photolysis (other experiments show more increase than Figure 5c), and decrease slightly on 25 K annealing. Using the HD reagent, the above bands were extremely weak, but new 1748.2 and 1232.1 cm^{-1} bands exhibited the same behavior (Figures 5 and 6). This is the pattern found for MnH_2 where the symmetric Mn−H stretching mode is above the antisymmetric Mn−H stretching mode, and the two new bands with HD confirm the identification of ReH_2. The unobserved symmetric stretching mode is predicted near 1850 cm^{-1}, substantially higher than the strong antisymmetric stretching mode.

The 1646.4 cm^{-1} assignment to the strong b_2 Re−H stretching fundamental of ReH_2 is supported by our DFT calculations, which find a slightly bent $^6A_1$ ground state with b_2 mode predicted at 1717.7 cm^{-1} (BPW91) and 1697.8 (B3LYP). Furthermore the much weaker, unobserved a_1 mode is predicted higher at 1874.5 cm^{-1} (BPW91) and 1871.8 cm^{-1} (B3LYP), in good agreement with extrapolation from the spectrum of ReHD. In addition, our BPW91 calculation predicts ReHD frequencies 85.9 and 45.9 cm^{-1} higher than ReH_2 and ReD_2, respectively, in very good agreement with the 101.8 and 49.5 cm^{-1} observed differences. It is possible that future higher level calculations will find ReH_2 to be linear; however, the strong infrared active fundamental should be observed at 1660 ± 10 cm^{-1} in the gas phase.

Our calculations find a bent quartet state slightly higher with BPW91 and slightly lower energy with B3LYP, but the b_2 frequency is above 2000 cm^{-1}. This is clearly not compatible with the observed spectrum of ReH_2.

ReH_4. The next most intense absorption in the argon matrix spectrum at 2037.2 cm^{-1} increased on annealing to 15 K, decreased on photolysis and increased on further annealing. With D_2 this band shifts to 1459.4 cm^{-1}, giving the 1.3959 H/D isotopic frequency ratio. The HD and $H_2 + D_2$ experiments gave doublets at 2037.2, 2043.8 cm^{-1} and 1460.0, 1465.0 cm^{-1}. This isotopic pattern of four Re−H(D) stretching modes is due to a tetrahydride species as described for ZrH_4, HfH_4,[20] WH_4,[25] and YH_4^-.[26] The above band pairs are assigned to symmetric and antisymmetric ReH_2 and ReD_2 stretching fundamentals, respectively, in ReH_2D_2. The Re−H and Re−D stretching frequencies of the tetrahydride are calculated by DFT (Table 6). The structure of ReH_4 is converged to D_{2d} symmetry instead of T_d, and as a result the degenerate ν_3 mode (t_2) in T_d symmetry is split into a b_2 mode at 2093.5 cm^{-1} and degenerate e mode at 2096.6 cm^{-1} with the BPW91 functional. However, one band

TABLE 7: Calculated Structures and Argon Matrix M−H Stretching Frequencies for the First Row Transition Metal Dihydrides[a]

	ScH_2	TiH_2	VH_2	CrH_2	MnH_2	FeH_2	CoH_2	NiH_2
ground state	$^2A_1$	$^3A_1$	$^4B_2$	$^5B_2$	$^6A_1$	$^5A_1$	$^4B_2$	$^1A_1$
M−H (Å)	1.815	1.749	1.692	1.638	1.669	1.620	1.566	1.425
HMH (deg)	116[b]	122	118	110	156[e]	146[f]	140	77
cal ν_3 (b_2)	1506	1578	1615	1663	1625	1694	1736	2119
cal ν_1 (a_1)	1528	1592	1639	1672	1691	1745	1800	2125
exp ν_3		1435[c]	1508[c]	1614[d]	1592[e]	1661[f]	1684[g]	1969[h]
exp ν_1			1532	1651				2007

[a] Calculated at BPW91/6-311++G(d,p) level. [b] Reference 26. [c] Xiao, Z. L.; Hauge, R. H.; Margrave, J. L. *J. Phys. Chem.* **1991**, *95*, 2696. See also ref 62. [d] References 17 and 55. [e] Reference 14, this work. MnH_2 is probably linear; see ref 53. [f] Reference 18. FeH_2 is probably linear; see ref 19. [g] Billups, W. E.; Chang, S.-C.; Hauge, R. H.; Margrave, J. L. *J. Am. Chem. Soc.* **1995**, *117*, 1387. [h] Reference 60.

observed at 2037.2 cm^{-1} for ReH_4 in solid argon, and the HD isotopic spectrum support approximate T_d symmetry. It is possible that the structure of ReH_4 is slightly distorted from T_d to D_{2d}, and that the band splitting is overestimated by theoretical calculations. Finally, a weaker 590.6 cm^{-1} band tracks with the 2037.2 cm^{-1} band in three experiments, and it is assigned to the strong bending mode predicted at 584.8 cm^{-1} by DFT.

Other Absorptions. Absorptions appeared on annealing at 1874.6 and 1848.4 cm^{-1} in solid argon. A neon counterpart was found at 1864.7 cm^{-1} and a pure deuterium counterpart at 1340.5 cm^{-1}. These bands are probably due to polymetal hydride species that cannot be identified. The observation[58] of stable ReH_9^{2-} at 1870 cm^{-1} and the strongest mode of ReH_2^- calculated at 2008 cm^{-1} by DFT further suggests that rhenium hydride molecular anions may be involved. Stable anions such as ReH_4^- and ReH_6^- have been computed.[59]

Bonding Considerations. As shown in Table 7 on the basis of the BPW91/6-311++G(d,p) calculations the MH_2 bond lengths decrease and the frequencies generally increase except for MnH_2 as atomic number increases. However, the bond angles for metal dihydrides are quite diverse. The early metal dihydrides (ScH_2, TiH_2, VH_2, and CrH_2) favor bond angles around 110−120°, but close-to-linear structures are found for MnH_2 (156°), FeH_2 (146°), and CoH_2 (141°). However, for NiH_2 the bond angle is reduced to 77°, which is in excellent agreement with recent observations and computations of the Weltner group for the $^1A_1$ state,[60] although the $^3\Delta_g$ state is found to be slightly lower in energy[61] and NiH_2 is thought to be linear from the photoelectron spectrum of NiH_2^-.[57] Different hybrid prototypes must be considered here.[47b] The optimal bond angles for sp and sd hybrids are 180° and 90°, respectively. For the early transition metals sd hybridization is more favorable but a mixture of 3d, 4s, and 4p is involved in the bonding. For MnH_2 sp hybridization is formed and the same bonding characters are expected for FeH_2 and CoH_2. In this case it seems d orbitals maintain high-spin, which retains a favorable exchange energy. Note a contamination from d character in the bonding orbital is not avoidable, which leads to a near-linear structure. By contrast, the bond angle is reduced to 77° in the $^1A_1$ state for NiH_2, in near agreement with other calculations,[52] indicating sd hybridization rather than sp, and more d than s character is involved in this bond. Recall that this bond angle is reduced to 29° for PdH_2, where no s orbital is involved and the molecule is essentially a $Pd(H_2)$ complex.[21]

Note that the antisymmetric frequency for the third row dihydride ReH_2 (1646 cm^{-1}) is higher than that for the first row dihydride MnH_2 (1592 cm^{-1} in argon). The same relationship is found for CrH_2 (1601 cm^{-1})[55] and WH_2 (1832 cm^{-1} in neon),[25] and for TiH_2 (1435 cm^{-1})[62] and HfH_2 (1622 cm^{-1} in argon).[20] This undoubtedly arises from the effect of relativistic contraction not counterbalanced by shell expansion, which lead to stronger bonds and higher vibrational frequencies for the third row hydrides.[63]

Reaction Mechanisms. Insertion of ground state Re into H_2 is exothermic by 12 kcal/mol (reaction 1) calculated at the BPW91 level, which is in near agreement with the CAS-MCSCF

$$\mathrm{Re}\ (^6S) + H_2 \rightarrow \mathrm{ReH_2}\ (^6A_1) \qquad \Delta E = -12\ \mathrm{kcal/mol} \quad (1)$$

prediction (18 kcal/mol);[10] however, reaction 1 is not spontaneous in this low-temperature matrix experiment. Theoretical calculations suggest that there is a large 100 kcal/mol energy barrier for this reaction, but that the a^6D excited state of the Re atom can avoid this barrier and insert into H_2.[10] In our experiments this insertion reaction is induced by broadband photolysis, which can access the a^6D excited state[64] near 14 200 cm^{-1}.

Similar insertion occurs in the manganese atom reaction with H_2, which is exothermic by 13 kcal/mol. Reaction 2 can be induced by $\lambda > 380$ nm photolysis, in solid neon. However, in

$$\mathrm{Mn}\ (^6S) + H_2 \rightarrow \mathrm{MnH_2}\ (^6A_1) \qquad \Delta E = -13\ \mathrm{kcal/mol} \quad (2)$$

solid argon, annealing to 20 K clearly increases the MnH_2 and MnD_2 absorptions. However, Ozin and McCaffrey[15] found that thermal Mn atoms co-deposited with H_2 in xenon gave no reaction product, but irradiation at 285 nm in the $^6P \leftarrow {}^6S$ resonance transition formed MnH_2. It is therefore likely that the growth of MnH_2 on annealing in solid argon is due to successive atom combination reactions 3 and 4 as MnH and MnH_2 are clearly formed on annealing.

$$\mathrm{Mn}\ (^6S) + \mathrm{H}\ (^2S) \rightarrow \mathrm{MnH}\ (^7\Sigma^+) \quad (3)$$

$$\mathrm{MnH}\ (^7\Sigma^+) + \mathrm{H}\ (^2S) \rightarrow \mathrm{MnH_2}\ (^6A_1) \quad (4)$$

The ReH_2 intermediate further reacts with H_2 to give ReH_4, reaction 5. This exothermic reaction proceeds spontaneously in the low-temperature matrix and shows no significant activation

$$\mathrm{ReH_2}\ (^6A_1) + H_2 \rightarrow \mathrm{ReH_4}\ (^2A_1) \qquad \Delta E = -26\ \mathrm{kcal/mol} \quad (5)$$

$$\mathrm{MnH_2}\ (^6A_1) + H_2 \rightarrow (H_2)\mathrm{MnH_2}\ (^4A_2) \qquad \Delta E = 15\ \mathrm{kcal/mol} \quad (6)$$

energy requirement. In contrast, a possible reaction channel of MnH_2 with H_2 to give $(H_2)MnH_2$ ($^4A_2$) is endothermic by 15 kcal/mol, and MnH_4 ($^2A_1$) lies 44 kcal/mol higher in energy. Accordingly, no further reaction of MnH_2 with H_2 was observed in neon, argon, and pure hydrogen, and MnH_2 is the dominant species. This is in marked contrast to CrH_2, which readily

complexes with dihydrogen.[54,55] In addition, we find with a 50/50 H_2/D_2 mixture that laser-ablated Mn reacts preferentially with H_2 as the MnH and MnH_2 bands are 4 times stronger than the MnD and MnD_2 absorptions. The small yield of MnHD shows that reaction 4 participates.

In the laser-ablation process the endothermic reaction of Re and Mn atoms with H_2 gives ReH and MnH, respectively, and these reactions are activated by excess energy in the laser-ablated metal atoms.[65]

$$\mathrm{Re}\ (^6\mathrm{S}) + \mathrm{H_2} \rightarrow \mathrm{ReH}\ (^5\Sigma) + \mathrm{H} \qquad \Delta E = 48\ \mathrm{kcal/mol} \quad (7)$$

$$\mathrm{Mn}\ (^6\mathrm{S}) + \mathrm{H_2} \rightarrow \mathrm{MnH}\ (^7\Sigma) + \mathrm{H} \qquad \Delta E = 54\ \mathrm{kcal/mol} \quad (8)$$

The MnH is trapped in argon, neon, and pure hydrogen, and a small amount of further reaction with H_2 is observed on annealing: reaction 9 is estimated to be exothermic at both BPW91 and B3LYP levels of theory. It is possible that reaction to form MnH_3 requires a large activation energy.

$$\mathrm{MnH}\ (^7\Sigma^+) + \mathrm{H_2} \rightarrow (\mathrm{H_2})\mathrm{MnH}\ (^5\mathrm{B_2}) \qquad \Delta E = -11\ \mathrm{kcal/mol} \quad (9)$$

Absorptions due to ReH and ReD are observed in solid argon; however, ReH_3 is not spectroscopically identified although reaction 10 is energetically feasible.

$$\mathrm{ReH}\ (^5\Sigma^+) + \mathrm{H_2} \rightarrow \mathrm{ReH_3}\ (^3\mathrm{A'}) \qquad \Delta E = -19\ \mathrm{kcal/mol} \quad (10)$$

Finally, the exothermic dimerizations of MnH and MnH_2 proceed although both appear to require activation by photolysis. In the case of MnH_2 a large reduction in MnH_2 angle accompanies the dimerization process. Our BPW91 calculations suggest a D_{2d} structure with a single Mn−Mn bond for Mn_2H_4.

$$2\mathrm{MnH}\ (^7\Sigma^+) \rightarrow (\mathrm{MnH})_2\ (^{11}\mathrm{A_g}) \qquad \Delta E = -46\ \mathrm{kcal/mol} \quad (11)$$

$$2\mathrm{MnH_2}\ (^6\mathrm{A_1}) \rightarrow \mathrm{Mn_2H_4}\ (^9\mathrm{X}) \qquad \Delta E = -13\ \mathrm{kcal/mol} \quad (12)$$

Conclusions

Manganese and rhenium atoms react with H_2 on condensation in excess neon, argon, and pure hydrogen and deuterium to form MH and MH_2 (M = Mn, Re) molecules, which are identified by D_2, HD, and $H_2 + D_2$ isotopic substitution on the observed fundamental frequencies. The diatomic molecule Mn−H absorbs at 1493.3 cm^{-1} (neon), 1486.4 cm^{-1} (pure hydrogen), and 1477.9 cm^{-1} (argon); however, ReH shows much higher vibrational frequency at 1985.0 cm^{-1} (argon). DFT calculations support the $^7\Sigma^+$ ground state for MnH whereas the ground state for ReH is predicted to be $^5\Sigma^+$.

The MnH_2 and ReH_2 molecules are identified from the effect of HD substitution on the spectra and the match of frequencies from DFT calculations. In addition, MnH_2^- is observed in solid neon.

The Mn_2H_4 molecule, formed in solid neon and hydrogen, is computed to have a nonet ground state D_{2d} structure with a Mn−Mn single bond.

The insertion reactions of Mn and Re into H_2 do not spontaneously happen in the low-temperature matrix environment even though these reactions are exothermic. However, spontaneous insertion reactions have been observed for Rh and Pt with hydrogen.[12,22] No further reactions were observed for MnH_2 with hydrogen, even in pure hydrogen, whereas ReH_2 combines with H_2 to give ReH_4, which is characterized by two infrared fundamentals and DFT calculations. This work reports the first experimental evidence for neutral rhenium hydride molecules.

Acknowledgment. We gratefully acknowledge support for this work from NSF Grant CHE00-78836 and helpful correspondence with C. W. Bauschlicher, Jr.

References and Notes

(1) Bravo, J. B.; Griswold, E.; Kleinberg, J. *J. Phys. Chem.* **1954**, *58*, 18.
(2) Abrahams, S. C.; Ginsberg, A. P.; Knox, K. *Inorg. Chem.* **1964**, *3*, 558.
(3) Huang, B.; Yvon, K.; Fischer, P. *J. Alloys Compounds* **1993**, *197*, 97.
(4) Stetson, N. T.; Yvon, K.; Fischer, P. *Inorg. Chem.* **1994**, *33*, 4598.
(5) Bronger, W.; Auffermann, G. *Z. Anorg. Allg. Chem.* **1999**, *625*, 1147.
(6) King, R. B. *Coord. Chem. Rev.* **2000**, *200*−*202*, 813 and references therein.
(7) Casey, C. P.; Underiner, T. L.; Vosejpka, P. C.; Gavney, J. A.; Kiprof, P. *J. Am. Chem. Soc.* **1992**, *114*, 10826.
(8) Albertin, G.; Antoniutti, S.; Garcia-Fontan, S.; Carballo, R.; Padoan, F. *J. Chem. Soc., Dalton Trans.* **1998**, *12*, 2071.
(9) Belkova, N. V.; Shubina, E. S.; Gutsul, E. I.; Epstein, L. M.; Eremenko, I. L.; Nefedov, S. E. *J. Organomet. Chem.* **2000**, *610*, 58.
(10) Dai, D.; Balasubramanian, K. *J. Chem. Phys.* **1991**, *95*, 4284 (Re+H_2).
(11) Balasubramanian, K.; Taio, D. *J. Phys. Chem.* **1988**, *92*, 6259.
(12) Wang, X.; Andrews, L. *J. Phys. Chem. A* **2002**, *106*, 3706 (Rh + H_2).
(13) Sweany, R. L. *Transition Metal Hydrides*; Dedieu, A., Ed.; VCH Publishers: New York, 1991.
(14) Van Zee, R. J.; DeVore, T. C.; Wilkerson, J. L.; Weltner, W., Jr. *J. Chem. Phys.* **1978**, *69*, 1869.
(15) Ozin, G. A.; McCaffrey, J. G. *J. Am. Chem. Soc.* **1984**, *106*, 807.
(16) Van Zee, R. J.; DeVore, T. C.; Weltner, W., Jr. *J. Chem. Phys.* **1979**, *71*, 2051.
(17) Xiao, Z. L.; Hauge, R. H.; Margrave, J. L. *J. Phys. Chem.* **1992**, *96*, 636 (Cr, Mo + H_2).
(18) Chertihin, G. V.; Andrews, L. *J. Phys. Chem.* **1995**, *99*, 1214 and references therein (Fe + H_2).
(19) (a) Körsgen, H.; Mürtz, P.; Lipus, K.; Urban, W.; Towle, J. P.; Brown, J. M. *J. Chem. Phys.* **1996**, *104*, 4859. (b) Körsgen, H.; Urban, W.; Brown, J. M. *J. Chem. Phys.* **1999**, *110*, 3861 (FeH_2).
(20) (a) Chertihin, G. V.; Andrews, L. *J. Am. Chem. Soc.* **1995**, *117*, 6402. (b) Chertihin, G. V.; Andrews, L. *J. Phys. Chem.* **1995**, *99*, 15004 (Zr, Hf + H_2).
(21) (a) Andrews, L.; Manceron, L.; Alikhani, M.; Wang, X. *J. Am. Chem. Soc.* **2000**, *122*, 11011. (b) Andrews, L.; Wang, X.; Alikhani, M.; Manceron, L. *J. Phys. Chem. A* **2001**, *105*, 3052 (Pd + H_2).
(22) Andrews, L.; Wang, X.; Manceron, L. *J. Chem. Phys.* **2001**, *114*, 1559 (Pt + H_2).
(23) Wang, X.; Andrews, L. *J. Am. Chem. Soc.* **2001**, *123*, 12899 (Au + H_2).
(24) Wang, X.; Andrews, L. *J. Phys. Chem. A* **2002**, *106*, 3744 (Au + H_2).
(25) (a) Wang, X.; Andrews, L. *J. Am. Chem. Soc.* **2002**, *124*, 5636. (b) Wang, X.; Andrews, L. *J. Phys. Chem. A* **2002**, *106*, 6720 (W + H_2).
(26) Wang, X.; Andrews, L. *J. Am. Chem. Soc.* **2002**, *124*, 7610 (Sc, Y, La + H_2).
(27) Burkholder, T. R.; Andrews, L. *J. Chem. Phys.* **1991**, *95*, 8697.
(28) Hassanzadeh, P.; Andrews, L. *J. Phys. Chem.* **1992**, *96*, 9177.
(29) Andrews, L.; Zhou, M.; Wang, X.; Bauschlicher, C. W. *J. Phys. Chem. A* **2000**, *104*, 8887 (Mn, Re + CO).
(30) Frisch, M. J.; Trucks, G. W.; Schlegel, H. B.; Scuseria, G. E.; Robb, M. A.; Cheeseman, J. R.; Zakrzewski, V. G.; Montgomery, J. A., Jr.; Stratmann, R. E.; Burant, J. C.; Dapprich, S.; Millam, J. M.; Daniels, A. D.; Kudin, K. N.; Strain, M. C.; Farkas, O.; Tomasi, J.; Barone, V.; Cossi, M.; Cammi, R.; Mennucci, B.; Pomelli, C.; Adamo, C.; Clifford, S.; Ochterski, J.; Petersson, G. A.; Ayala, P. Y.; Cui, Q.; Morokuma, K.; Malick, D. K.; Rabuck, A. D.; Raghavachari, K.; Foresman, J. B.; Cioslowski, J.; Ortiz, J. V.; Stefanov, B. B.; Liu, G.; Liashenko, A.; Piskorz, P.; Komaromi, I.; Gomperts, R.; Martin, R. L.; Fox, D. J.; Keith, T.; Al-Laham, M. A.; Peng, C. Y.; Nanayakkara, A.; Gonzalez, C.; Challacombe, M.; Gill, P. M. W.; Johnson, B. G.; Chen, W.; Wong, M. W.; Andres, J. L.; Head-Gordon,

M.; Replogle, E. S.; Pople, J. A. *Gaussian 98*, revision A.6; Gaussian, Inc.: Pittsburgh, PA, 1998.

(31) Becke, A. D. *Phys. Rev. A* **1988**, *38*, 3098.

(32) Perdew, J. P.; Wang, Y. *Phys. Rev. B* **1992**, *45*, 13244.

(33) Becke, A. D. *J. Chem. Phys.* **1993**, *98*, 5648.

(34) Lee, C.; Yang, E.; Parr, R. G. *Phys. Rev. B* **1988**, *37*, 785.

(35) Krishnan, R.; Binkley, J. S.; Seeger, R.; Pople, J. A. *J. Chem. Phys.* **1980**, *72*, 650. McLean, A. D.; Chandler, G. S. *J. Chem. Phys.* **1980**, *72*, 5639. Frisch, M. J.; Pople, J. A.; Binkley, J. S. *J. Chem. Phys.* **1984**, *80*, 3265.

(36) Wachters, A. J. H. *J. Chem. Phys.* **1970**, *52*, 1033. Hay, P. J. *J. Chem. Phys*. **1977**, *66*, 4377. Raghavachari, K.; Trucks, G. W. *J. Chem. Phys.* **1989**, *91*, 1062.

(37) Andrae, D.; Haussermann, U.; Dolg, M.; Stoll, H.; Preuss, H. *Theor. Chim. Acta* **1990**, *77*, 123.

(38) Zhou, M.; Zhang, L.; Shao, L.; Wang, W.; Fan, K.; Qin, Q. *J. Phys. Chem. A* **2001**, *105*, 5801.

(39) Chertihin, G. V.; Andrews, L. *J. Phys. Chem. A* **1997**, *101*, 8547 ($Mn + O_2$).

(40) Milligan, D. E.; Jacox, M. E. *J. Mol. Spectrosc.* **1973**, *46*, 460. Andrews, L.; Ault, B. S.; Grzybowski, J. M.; Allen, R. O. *J. Chem. Phys.* **1975**, *62*, 2461.

(41) Zhou, M. F.; Citra, A.; Liang, B.; Andrews, L. *J. Phys. Chem. A* **2000**, *104*, 3457 ($Re + O_2$).

(42) Huber, K. P.; Herzberg, G. *Constants of Diatomic Molecules*; Van Nostrand Reinhold: New York, 1979.

(43) Urban, R. D.; Jones, H. *Chem. Phys. Lett.* **1989**, *163*, 34; **1991**, *178*, 295.

(44) Varberg, T. D.; Field, R. W.; Merer, A. J. *J. Chem. Phys.* **1990**, *92*, 7123.

(45) Balfour, W. J.; Lindgren, B.; Launila, O.; O'Connor, S.; Cusack, E. J. *J. Mol. Spectrosc.* **1992**, *154*, 177 and references therein.

(46) Verberg, T. D.; Gray, J. A.; Field, R. W.; Mercer, A. J. *J. Mol. Spectrosc.* **1992**, *156*, 296 and references therein.

(47) (a) Chong, D. P.; Langhoff, S. P.; Bauschlicher, C. W., Jr.; Walch, S. P.; Partridge, H. *J. Chem. Phys.* **1986**, *85*, 2850. (b) Bauschlicher, C. W.; Langhoff, S. R. *Transition Metal Hydrides*; Dedieu, A.. Ed; VCH Publishers: New York, 1991.

(48) Harrison, J. F. *Chem. Rev.* **2000**, *100*, 679 and references therein.

(49) Witborn, C.; Wahlgren, U. *Chem. Phys.* **1995**, *201*, 357.

(50) Dai, D.; Balasubramanian, K. *J. Mol. Spectrosc.* **1993**, *158*, 455.

(51) Demuynck, J.; Schaefer, H. F., III. *J. Chem. Phys.* **1980**, *72*, 311.

(52) Platts, J. A. *J. Mol. Struct. (THEOCHEM)* **2001**, *545*, 111.

(53) Balabanov, N. B.; Boggs, J. E. *J. Phys. Chem. A* **2002**, *106*, 6839.

(54) Ma, B.; Collins, C. L.; Schaefer, H. F., III. *J. Am. Chem. Soc.* **1996**, *118*, 870.

(55) Wang, X.; Andrews, L. *J. Phys. Chem. A* **2003**, *107*, 570.

(56) Jacox, M. E. *Chem. Phys.* **1994**, *189*, 149.

(57) Miller, A. E.; Feigerle, C. S.; Lineberger, W. C. *J. Chem. Phys.* **1986**, *84*, 4127.

(58) Stetson, N. T.; Yvon, K.; Fischer, P. *Inorg. Chem.* **1994**, *33*, 4598.

(59) Bayse, C. A.; Hall, M. B. *J. Am. Chem. Soc.* **1999**, *121*, 1348.

(60) Li, S.; Van Zee, R. J.; Weltner, W., Jr.; Cory, M. G.; Zerner, M. C. *J. Chem. Phys.* **1997**, *106*, 2055.

(61) Blomberg, M. R. A.; Siegbahn, P. E. M. *J. Chem. Phys*. **1983**, *78*, 5682 (NiH_2).

(62) Chertihin, G. V.; Andrews, L. *J. Am. Chem. Soc.* **1994**, *116*, 8322.

(63) Pyykko, P. *Chem. Rev.* **1988**, *88*, 563.

(64) Moore, C. E., *Atomic Energy Levels*; National Bureau of Standards: Washington, DC, 1952; Vol. II.

(65) Kang, H.; Beauchamp, J. L. *J. Phys. Chem.* **1985**, *89*, 3364.